Electronic Supporting Information

Near-infrared-II Thermally Activated Delayed Fluorescent Organic Light-emitting Diodes

Qingxin Liang [†, a], Jingyi Xu [†, a], Jie Xue [a, b, *] and Juan Qiao [a, b, *]

[a] Department of Chemistry, Key Lab of Organic Optoelectronics and Molecular Engineering of Ministry of Education, Tsinghua University, Beijing 100084, China. E-mail: *qjuan@mail.tsinghua.edu.cn; xuejie@mail.tsinghua.edu.cn*
[b] Center for Flexible Electronics Technology, Tsinghua University, Beijing 100084, P. R. China.
[†] These authors contribute equally to this work.

Material Synthesis and Characterizations

TPAAZ was synthesized through Suzuki reaction and condensation reactions according to previous reports.[1] All purchased reagents were analytical pure without further purification. 5-(4-(diphenylamino)phenyl)acenaphthylene-1,2-dione was synthesized according to literature.[1]

600 MHz ^{1}H-NMR and 150 MHz ^{13}C-NMR spectra were measured by a JEOL JNM-ECS600 spectrometer at room temperature in deuterated dichloromethane and chloroform respectively with tetramethyl silane as the internal standard. MALDI-TOF-MS data was performed on a Shimadzu AXIMA Performance MALDI-TOF instrument in positive detection modes. Elemental analysis was obtained with a CE-440 Elemental Analyzer.

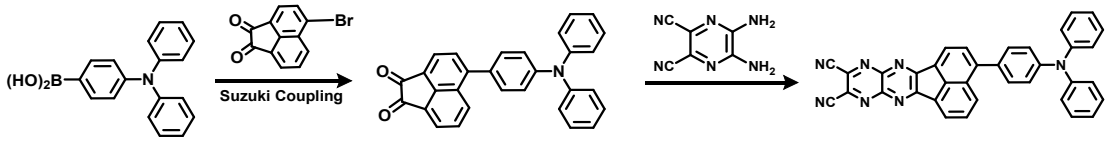

Scheme S1. Synthetic procedure of TPAAZ.

3-(4-(diphenylamino)phenyl)acenaphtho[1,2-b]pyrazino[2,3-e]pyrazine-9,10-dicarbonitrile (TPAAZ):

5-(4-(diphenylamino)phenyl)acenaphthylene-1,2-dione (1.0 g, 2.4 mmol) and 5,6-diaminopyrazine-2,3-dicarbonitrile (0.56 g, 3.5 mmol) were dissolved in a 500 mL round-bottle flash with 300 mL glacial acetic acid. Under nitrogen atmosphere, the mixture was stirred under reflux with the temperature of 130℃ for 24 hours. After condensation reaction, the cooled solution was treated with extraction filtration to remove solvents, then the filter cake was washed by a small amount of acetone, ethanol

and deionized water to remove the residuals. The separated solid was further baked for 12 hours in vacuum oven. The gross product was purified by using column chromatography with dichloromethane and petroleum ether at a volume ratio of 7:1 as the eluent to give a deep-purple solid (1.10 g, yield: 85%). This solid was further purified through temperature gradient vacuum sublimation under the temperature of 240-260℃ and atmospheric pressure of 7×10^{-4} Pa.

^{1}H-NMR (CD_2Cl_2, 600 MHz) δ(ppm): 8.70 (dd, *J* = 7.1, 1.6 Hz, 2H), 8.58 (d, *J* = 8.4 Hz, 1H), 8.00 (m, 2H), 7.56 (d, *J*=8.5 Hz, 2H), 7.33 (t, *J* = 7.9Hz, 4H), 7.22 (m, 6H), 7.11 (t, *J* = 7.3 Hz, 2H). ^{13}C-NMR ($CDCl_3$, 150 MHz) δ(ppm): 162.13, 161.32, 149.05, 147.19, 145.42, 145.12, 141.33, 132.56, 131.93, 131.54, 131.08, 130.80, 130.04, 129.67, 129.55, 128.73, 128.57, 126.89, 126.14, 125.84, 125.42, 124.08, 122.34, 112.95. MALDI-TOF-MS: m/z calcd, $[M]^+$ = 549.17, found, $[M]^+$ = 549.18. Elemental analysis calculated for $C_{36}H_{19}N_7$: C, 78.68%, H, 3.48%, N, 17.84%. Found: C, 78.25%, H, 3.58%, N, 17.49%.

Single Crystal

The single crystals were obtained during vacuum sublimation. The structure was measured by the low temperature (104.6K) single-crystals X-ray experiments with a Rigaku RAXIS-SPIDER IP diffractometer and solved by the Rigaku RAPID AUTO software package (Rigaku, 1998, Version 2.30). The crystallographic data can be obtained free of charge from The Cambridge Crystallographic Data Centre via www.ccdc.cam.ac.uk/data_request/cif. with CCDC 1996161.

Thermal Analysis

Thermogravimetric analyses (TGA) was carried out on a STA 409PC thermogravimeter by measuring the weight loss from room temperature to 700 °C under nitrogen atmosphere. The heating rate was 10 °C min^{-1}. The decomposition temperature (T_d) was the temperature related to the 5% weight loss. Differential scanning calorimetry (DSC) measurements were conducted on a TA Instruments DSC 2910 modulated calorimeter under nitrogen atmosphere from 25 °C to 380 °C. The heating rate was 5 °C min^{-1} The glass transition temperature (T_g) was measured with the first exothermic peak.

Electrochemical Analysis

The experimental HOMO and LUMO energy were measured with cyclic voltammetry method with a CHI 600E electrochemical workstation. The working electrode is a platinum disk electrode, the auxiliary electrode is a platinum wire, and the reference electrode is silver wire. All the electrodes were polished and cleaned before measurement. 5.0 mg TPAAZ were solved in 10.0 mL anhydrous N, N-dimethylformamide (DMF), then 0.4 g tetrabutylammonium hexafluorophosphate (n-Bu_4NPF_6) were added as supporting electrolyte. After deoxygenation with nitrogen bubbles for 10 minutes, the oxidation and reduction potential were measured at a scan rate of 100 mV·s^{-1}. Then ferrocene was added to the solution in order to standardize zero vacuum level with ferrocene/ferrocenium (Fc/Fc^+) potential.

Photoluminescence Property Measurement

1×10^{-5} M solutions were prepared with 100 mL volumetric flask for all the solution measurements. Pure TPAAZ films and TPAAZ:CBP doped films were vacuum evaporated on quartz substrates. Absorption spectra were measured with an Agilent 8453 UV-vis spectrophotometer. Emission spectra and transient spectra were collected on an Edinburgh Fluorescence Spectroscopy FLS920 equipped with a R928P photomultiplier tube (200-900 nm, often fail to detect the certain spectra after 800 nm) and a Hamamatsu R5509 near infrared photomultiplier tube. Fluorescent spectra were collected with a xenon lamp. The phosphorescent spectra were collected with a 60 W μF2 microflash lamp, R928P photomultiplier tube and multi-channel scanning counting technique after gating for 0.5 ms in Oxford DN2 liquid nitrogen cryostat at 77K. The energy of S_1 state were estimated from the onset of the absorption spectra, while the ΔE_{ST} were estimated from the onset of the fluorescent spectra at 77K for S_1 state energy and phosphorescent spectra for T_1 state energy, respectively. Both the solution samples and film samples were deoxygenated with nitrogen bubbling and vacuum pumping respectively before transient spectra collections. Transient spectra for prompt part were collected with a 442 nm picosecond pulsed LED (EPL450), while the delayed parts were collected with a 447 nm pulse width tuning laser (VPL450) for film and a μF2 microflash lamp for solution. The PLQYs were obtained with an absolute photoluminescence quantum yield measurement system Hamamatsu C9920-03G in an integrating sphere. The solution sample was bubbled with nitrogen for 10 minutes before measurement while the films were measured in air.

Lifetime (τ_i) and the corresponding pre-exponential (A_i) were calculated with F900 program comes with the FLS920 spectroscopy. Then the average lifetime (τ_{av}) was calculated as $\tau_{av} = \sum A_i\tau_i^2/\sum A_i\tau_i$. The prompt ($\tau_p$) and delayed lifetime ($\tau_{TADF}$) in the paper are average lifetime.

The percentage of delayed fluorescence is calculated by comparing the integrated transient decay spectra of delayed fluorescence and the whole fluorescence.[2] Then the PLQY of prompt fluorescence (Φ_p) and the delayed fluorescence (Φ_{TADF}) are calculated with the total PLQY and the percentage of delayed fluorescence.

The radiative rate constant (k_r), non-radiative rate constant (k_{nr}), inter-system crossing rate constant (k_{ISC}), thermally activated delayed fluorescence rate constant (k_{TADF}) and reverse intersystem crossing (k_{RISC}) are calculated with the formulas below[1-3]:

$$k_r = \phi_p/\tau_p$$

$$\phi = k_r/(k_r + k_{nr})$$

$$\phi_p = k_r/(k_r + k_{nr} + k_{ISC})$$

$$\phi_{ISC} = k_{ISC}/(k_r + k_{nr} + k_{ISC})$$

$$k_{RISC} = k_r \times k_{TADF} \times \phi_{TADF}/(k_{ISC} \times \phi_p)$$

Device Fabrication and Characterization

The ITO-coated glass substrates were purchased from Suzhou Fangsheng Optoelectronics co. LTD. TPAAZ were sublimated before use and all the other organic materials were purchased from Xi'an Polymer Light Technology Cooperation. The LiF powder were purchased from Alfa Aesar with Puratronic brand. The 99.999% aluminum blocks were purchased from Beijing China New Metal Limited Company.

The ITO substrates were cleaned with ultrasound in detergent, distilled water, acetone, isopropanol, boiled distilled water in turn then dried in drying oven at 100℃. Before vacuum evaporation, ITO substrates were treated with UV ozone for 10 min. Once the vacuum degree of the evaporating cave reaches 2×10^{-4} Pa, organic materials were evaporated at a rate of 1-2 Å/s, then the LiF was evaporated at a rate of 0.2 Å/s and aluminum at 2-3 Å/s. Devices were taken out from the dry nitrogen glove box and then measured in air as soon as possible.

The current density, voltage, radiant flux, EQE, electroluminescent spectra and other characteristics were measured with a Keithley 2400 source meter and an absolute EQE measurement system in an integrating sphere at the same time. The EQE measurement system is Hamamatsu C9920-12, which equipped with Hamamatsu PMA-12 Photonic multichannel analyzer C10027-02 whose longest detection wavelength is 1100 nm.

Theoretical Calculations

The Gaussian 16 program package[4] was used for all of the calculations.

Theoretical Calculations of Monomers:

The optimization and calculation of the ground state were performed on Gaussian package by density functional theory (DFT) with the B3LYP functional and 6-31g(d) basis set in gas phase based on the original geometrical configurations in the single crystal.

The calculation of excited state energy was based on the optimized ground state structure. The energy, the frontier molecular orbitals (FMO) and the natural transition orbitals (NTO) of the excited states were performed with the time-dependent DFT (TDDFT) using the B3LYP functional with 6–31G(d) basis set in gas phase.

The calculation of spin-orbital coupling (SOC) matrix elements was based on the optimized S_1 state structure in the gas phase with B3LYP functional and 6–31G* basis. Frequencies and structure optimization were calculated with Gaussian 16, and Multiwfn 3.7 Package[5] was used for the transformation of input files. Then the SOC matrix elements were calculated with Dalton 2018.2 program[6]. The sum of SOC matrix element in the whole space was based on the geometric mean of the three SOC matrix elements in x, y, z directions in the output file.

Theoretical Calculations of Dimers:

There were 18 closely packed dimers in the single crystal where there are intermolecular interactions between the two molecules. After the TDDFT calculations based on B3LYP functional with 6–31G(d) basis set in gas phase, dimer **1**, **2, 7, 8, 9, 10** with relatively low S_1 state energy were picked out for further calculations and analysis.

To describe the aggregation state, the calculations on the 6 dimers with the relatively low S_1 energies were conducted based on combined quantum mechanics and molecular mechanics (QM/MM) method with two-layer ONIOM method. The dimer was treated as QM region (high layer) with B3LYP/6-31g(d), while the other 40 molecules around the dimer in the crystal were frozen as MM region (low layer) with universal force field (UFF).[1] The excited states energies were calculated by TDDFT at B3LYP/6-31g(d) based on optimized ground state structure in QM/MM model and listed in Table S5. Then the hole and electron distributions were calculated with Multiwfn. The calculation of SOC matrix elements of dimers were not conducted because we failed to optimize the structures of the excited states.

Calculations of CT contributions:

The CT contributions were calculated with 'InterFragment Charge Transfer (IFCT)' method with Multiwfn 3.7 package.[5,7,8] The IFCT method contains three steps. The first is to calculate the atomic contribution to hole and electron,[7a] then sum up them to the fragments ($\Theta_{D,hole}$, $\Theta_{A,hole}$, $\Theta_{D,elecron}$, $\Theta_{A,elecron}$).[7b] Thus, all of the molecular orbitals that contribute to the excitation can be included in the calculation. The interfragment charge transfer matrix Q of the energy transfer from D to A fragments will be:[7b] $Q_{D,A} = \Theta_{D,hole}\Theta_{A,electron}$. The net electron transfer from D to A will be: [7b]$p_{D\rightarrow A} = Q_{D,A} - Q_{A,D}$.

The NTO analysis for S_1 and T_1 states of monomer were performed by TDDFT with B3LYP/6-31g(d) based on the optimized ground state structure, while the excited states of dimers were based on the optimized ground state structure from the QM/MM models. The IOp(9/40=3) command is contained during calculation so that all configuration coefficients whose magnitude larger than 0.001 will be printed.[7c] After calculations according to the manual,[7d] the net electron transfer from D to A will be output. We treat this net electron transfer in percentage as the CT contributions. For monomers, the D and A fragments are the donor and acceptor part of TPAAZ, respectively, and the CT contributions represent the net charge transfer ratio from donor to acceptor. For dimers, the D and A fragments are just the two molecules, and the intermolecular CT contributions were calculated from the sum of the intermolecular charge transfer ratio.

Table S1. Photophysical properties of TPAAZ in toluene solution

λ_{abs} [nm]	λ_{em} [nm]	E_{S1}[c] [eV]	E_{T1}[d] [eV]	ΔE_{ST} [eV]	PLQY	τ [ns]	k_r [$\times 10^7$ s^{-1}]	k_{nr} [$\times 10^8$ s^{-1}]
348[a]/394[a]/ 468[a] /613[b]	607[b]/742[a]	2.04	1.97	0.07	7.7%	3.55	2.17	2.60

[a] Peak wavelength. [b] Onset Wavelength. [c] Calculated from emission onset at 77 K. [d] Calculated from emission onset of phosphorescence at 77K.

Table S2. Photophysical properties of TPAAZ films doped in CBP

Doping conc. [wt]	Φ_{PL} [%]	TADF ratio [%]	Φ_p [%]	Φ_{TADF} [%]	k_r [$\times 10^6$ s^{-1}]	k_{nr} [$\times 10^7$ s^{-1}]	k_{ISC} [$\times 10^7$ s^{-1}]	k_{TADF} [$\times 10^2$ s^{-1}]	k_{RISC} [$\times 10^1$ s^{-1}]
1%	10.7	77.1	2.45	8.25	2.24	1.87	7.54	6.37	6.83
10%	4.2	86.3	0.58	3.6	1.25	2.85	18.7	112	46.8

Table S3. Calculated properties of TPAAZ monomer.

excited state	E [eV]	λ [nm]	f	μ_D (D)	CT contribution [a]	FMOs [b]
S_1	1.8052	686.81	0.0716	51.8	86.0%	H→L
S_2	2.1589	574.29	0.3296	44.5	37.4%	H→L+1
						H→L 90.8%
T_1	1.7104	724.87	0.0000	47.8	63.0%	H→L+1 5.5%
						H-1→L 3.7%

[a] CT contribution = the net electron transfer ratio from TPA donor to AZ acceptor.

[b] FMO = Frontier Molecular Orbitals, H = HOMO, L = LUMO.

Table S4. Calculated properties of TPAAZ dimers in gas phase.

dimer	E_{S1} (eV)	E_{T1} (eV)	f_{s1}	λ_{S1} (nm)	ΔE_{ST} (eV)
1	1.0778	1.0777	0.0001	1150.38	0.0001
2	1.3361	1.2784	0.0398	927.95	0.0577
3	1.8338	1.7516	0.0103	676.09	0.0822
4	1.9558	1.8115	0.0048	633.92	0.1443
5	1.8419	1.7355	0.1007	673.12	0.1064
6	1.9368	1.8113	0.0571	640.16	0.1255
7	1.2191	1.2095	0.0000	1017.03	0.0096
8	1.3326	1.3057	0.0001	930.41	0.0269
9	1.4060	1.3622	0.0000	881.83	0.0438
10	1.6182	1.5106	0.1816	766.19	0.1076
11	1.9230	1.7660	0.1167	644.73	0.1570
12	1.8653	1.7533	0.0711	664.69	0.1120
13	1.8820	1.7700	0.0754	658.79	0.1120
14	1.8675	1.7573	0.1006	663.91	0.1102
15	1.8232	1.7187	0.0998	680.05	0.1045
16	1.8820	1.7700	0.0754	658.79	0.1120
17	1.9625	1.7994	0.0835	631.78	0.1631
18	1.7248	1.6700	0.0000	718.83	0.0548

Table S5. Calculated properties of TPAAZ dimers with QM/MM method.

dimer	E_{S1} (eV)	E_{T1} (eV)	f_{s1}	λ_{S1} (nm)	ΔE_{ST} (eV)
1	1.1555	1.1554	0.0001	1072.95	0.0001
2	1.1735	1.1441	0.0109	1056.51	0.0294
7	1.2560	1.2436	0.0026	987.12	0.0124
8	1.2024	1.1628	0.0000	1031.15	0.0396
9	1.3448	1.2773	0.0003	921.98	0.0675
10	1.4373	1.3245	0.0992	862.63	0.1128

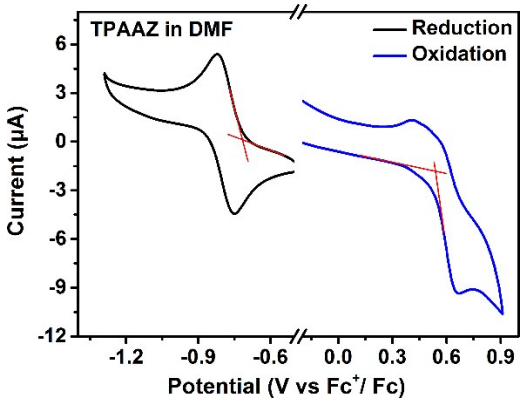

Fig. S1. Cyclic voltammograms curves of TPAAZ versus Fc/Fc^{+}.

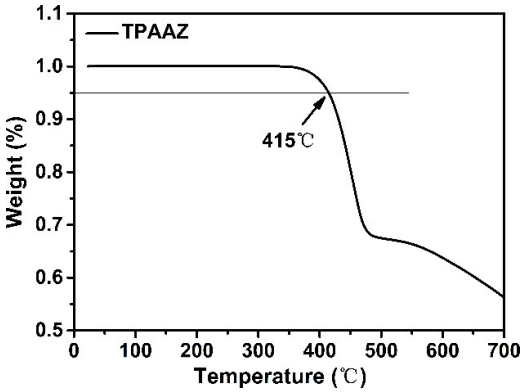

Fig. S2. Thermogravimetric analysis (TGA) curves of TPAAZ.

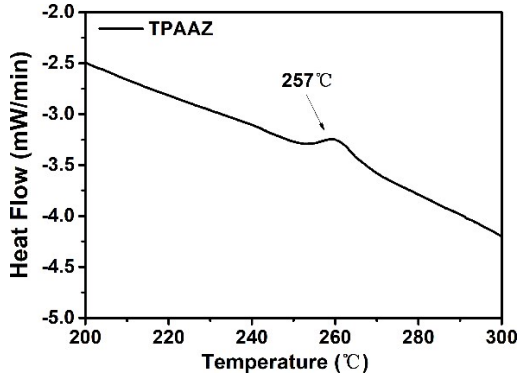

Fig. S3. Differential scanning calorimetry (DSC) curves of TPAAZ.

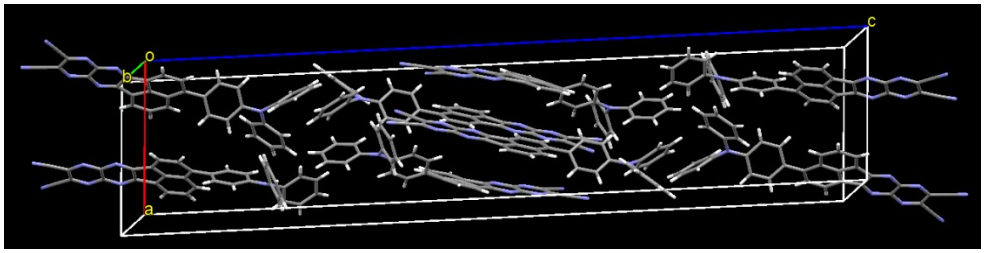

Fig.S4. Single crystal of TPAAZ.

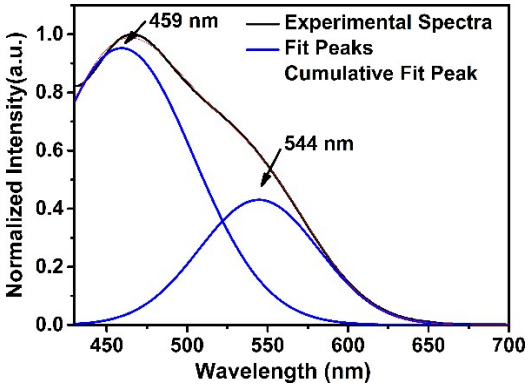

Fig. S5. Analysis of the TPAAZ absorption curve in toluene with Gauss function in Origin 9.2.

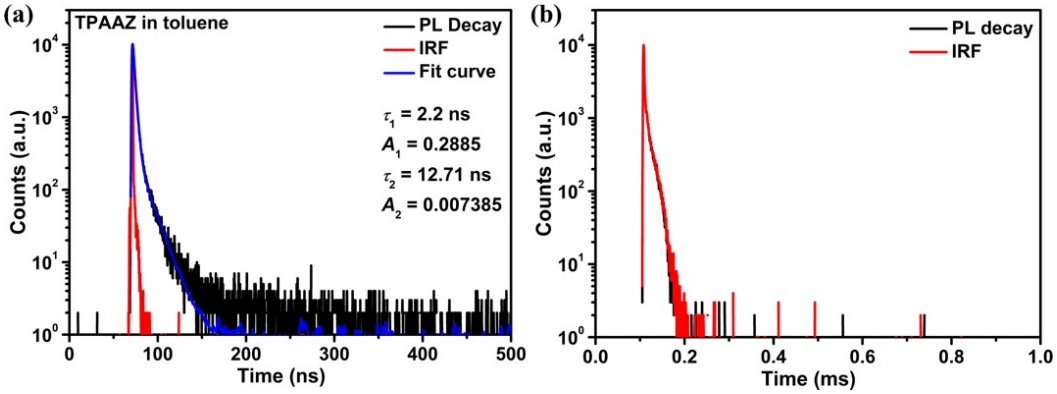

Fig. S6. Transient decay curve of TPAAZ in toluene. (a) Prompt curve. (b) Delayed curve. There is no delayed component in the curve.

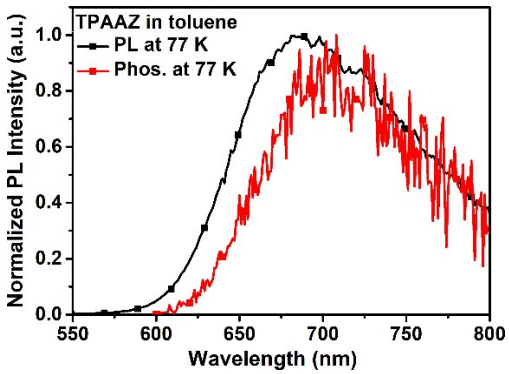

Fig. S7 PL spectra of TPAAZ in toluene at 77 K.

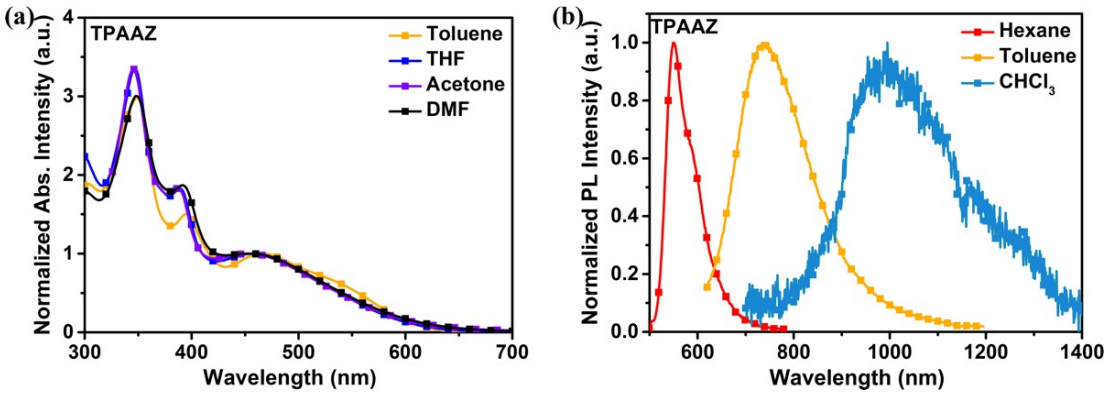

Fig. S8. Absorption (a) and emission (b) spectra of TPAAZ in different solvents: n-hexane (Hexane), toluene, chloroform ($CHCl_3$), tetrahydrofuran (THF), acetone and DMF. The emission spectra were too weak to detect in THF, acetone and DMF.

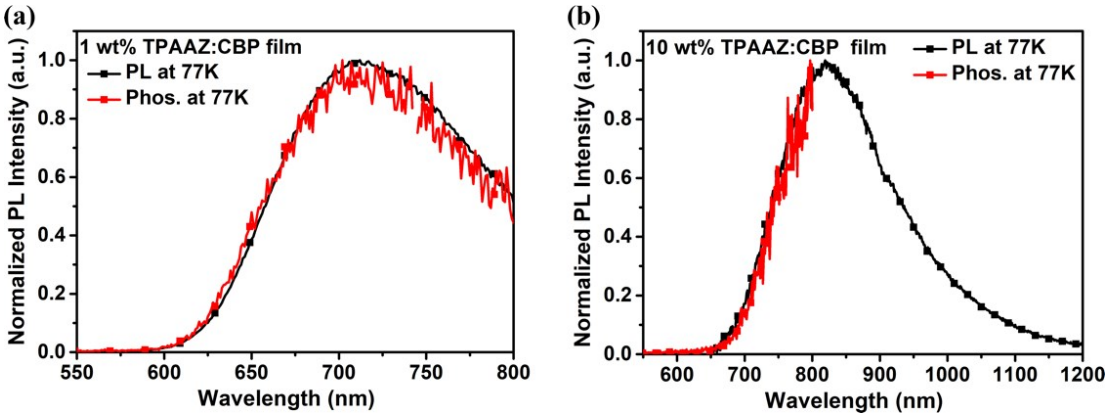

Fig. S9. Fluorescent spectra (black) and phosphorescent spectra (red) of 1 wt% (a) and 10 wt% (b) TPAAZ:CBP film at 77K. The 10 wt % phosphorescent spectra are fragmentary because of the poor response of R982P detector beyond 800 nm.

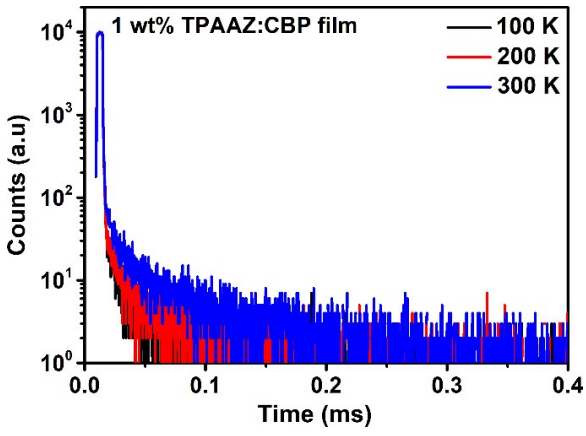

Fig. S10. Temperature dependent transient decay curve of 1 wt% TPAAZ:CBP film.

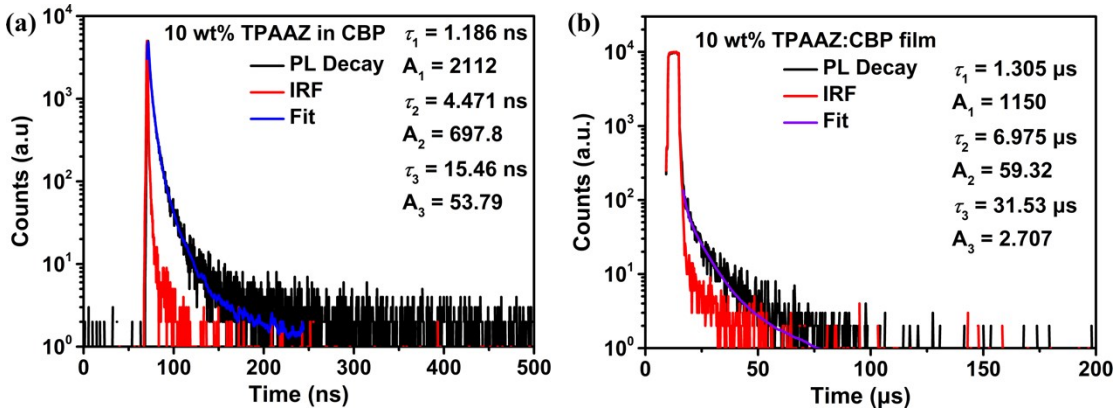

Fig. S11. Transient decay curve of 10 wt% TPAAZ:CBP film. (a) Prompt curve. (b) Delayed curve.

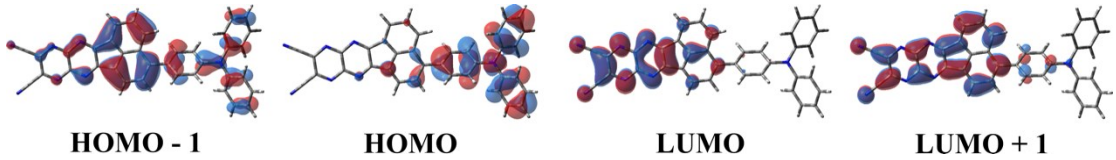

Fig. S12. Frontier molecular orbitals of TPAAZ monomer. Isovalue = 0.02.

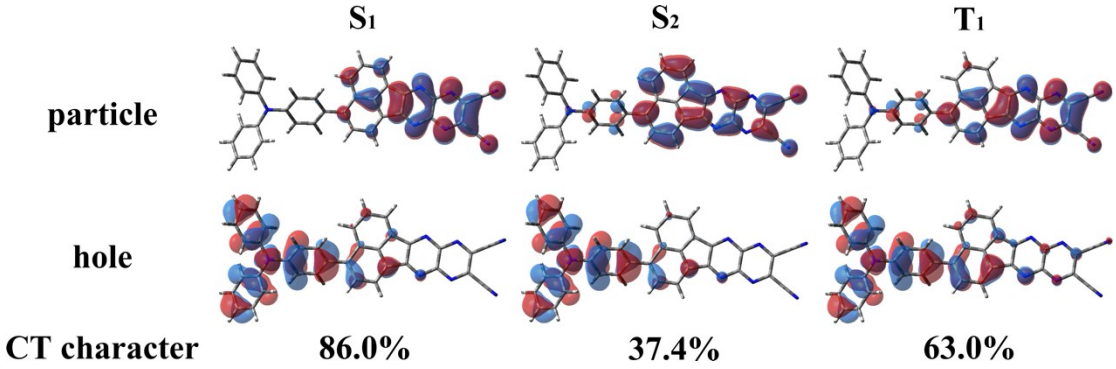

Fig. S13. NTOs of TPAAZ at S_1, S_2, T_1 states and their CT contributions.

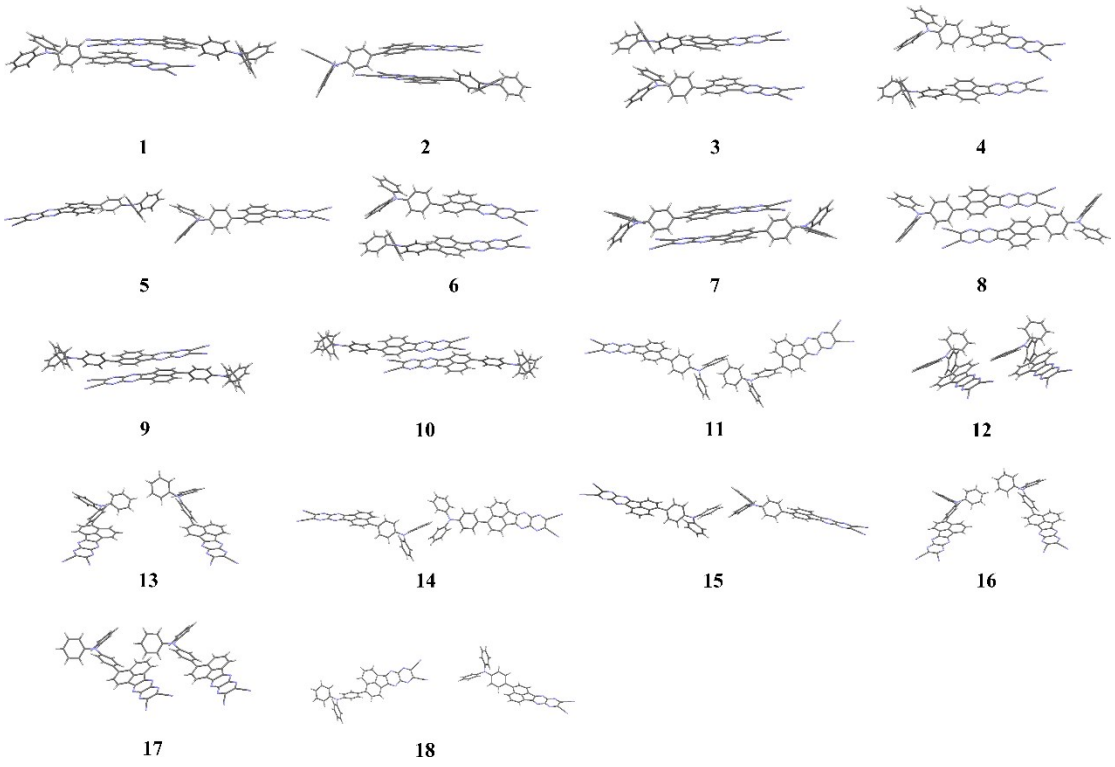

Fig. S14. Packing modes of TPAAZ dimers.

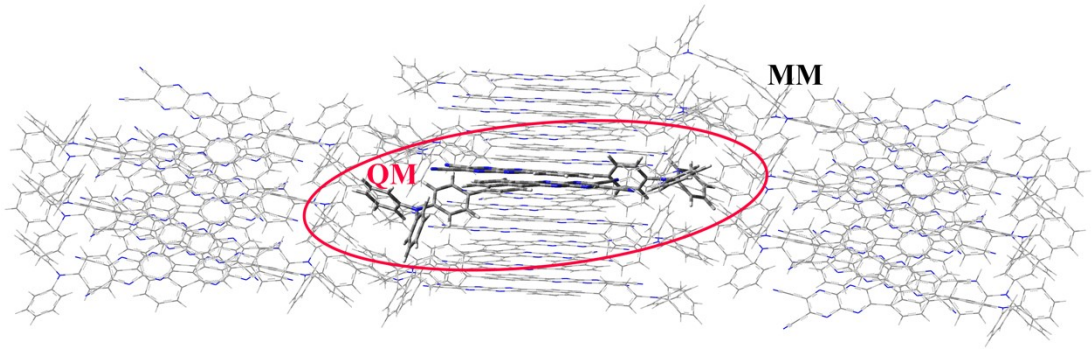

Fig. S15 Packing modes of the optimized dimer **1**

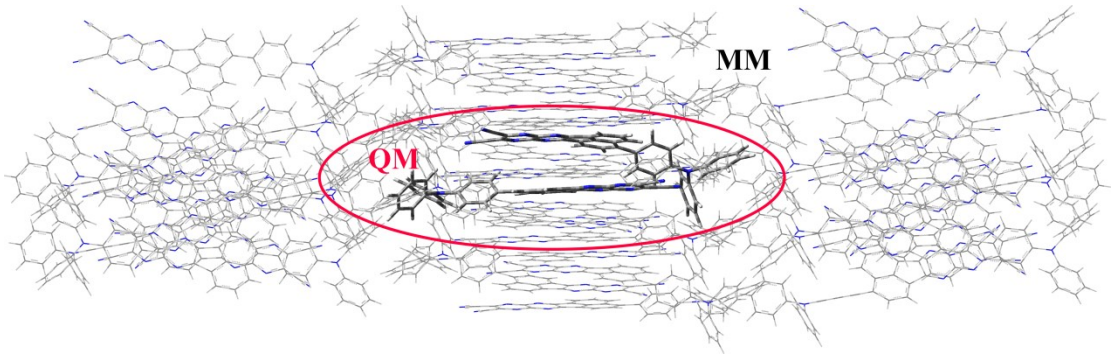

Fig. S16 Packing modes of the optimized dimer **2**

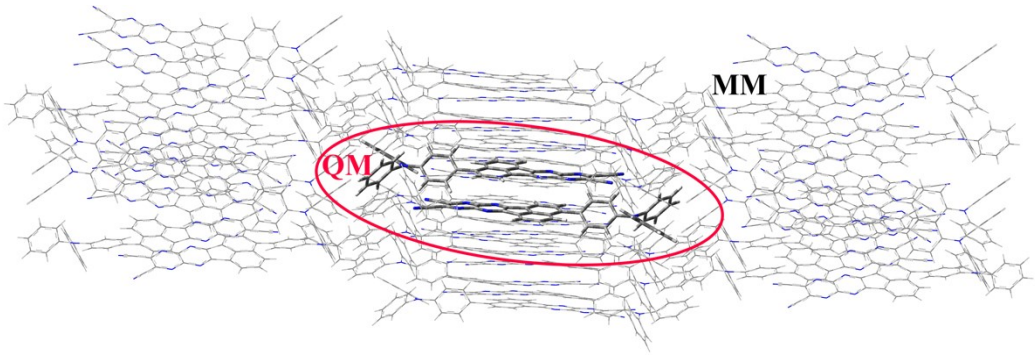

Fig. S17 Packing modes of the optimized dimer **7**

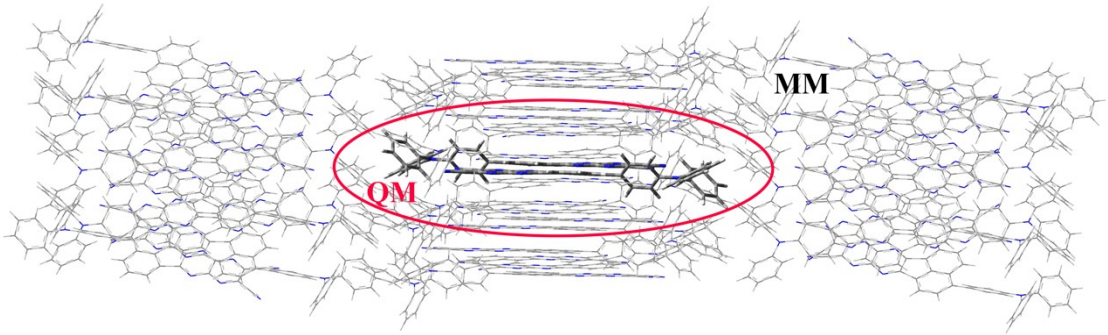

Fig. S18 Packing modes of the optimized dimer **8**

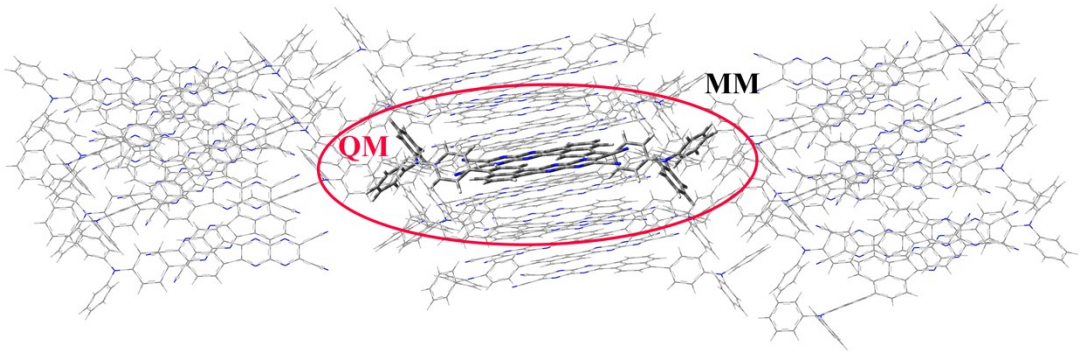

Fig. S19 Packing modes of the optimized dimer **9**

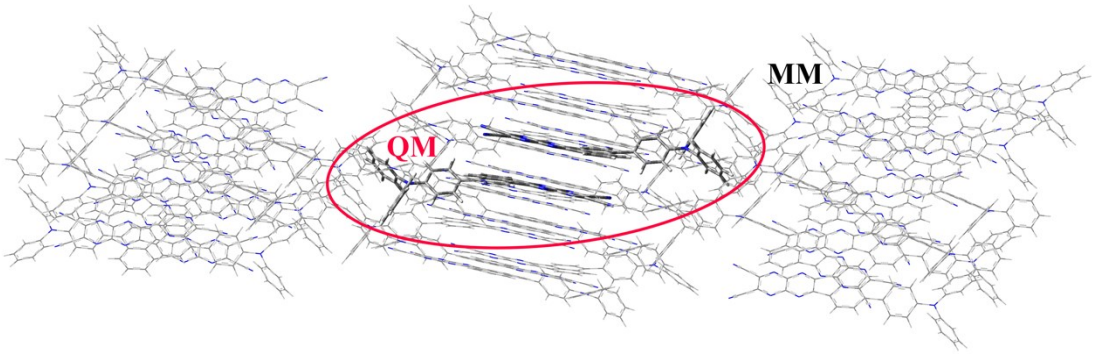

Fig. S20 Packing modes of the optimized dimer **10**

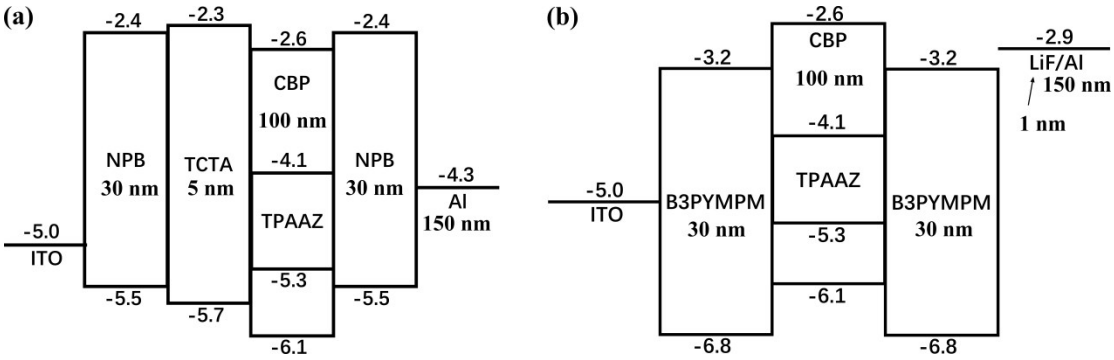

Fig. S21 Single carrier device structures with energy levels (unit: eV): (a) single hole device (b) single electron device

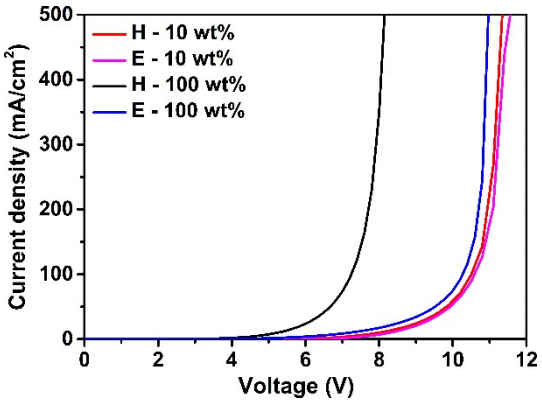

Fig. S22 Current density-voltage characteristics of single carrier devices. H: single-hole device. E：single-electron device. 1 wt%: 1 wt% TPAAZ:CBP as emitting layer. 100 wt%: TPAAZ as emitting layer.

The current density of both the single-hole device (blue) and the single-electron device (black) of the non-doped films increase faster than the doped ones as the voltage increase, which agrees well with the OLEDs (Fig. 4c), so a better charge-injecting / transporting ability of the non-doped emitting layer leads to the higher current density at the same voltage in OLEDs.

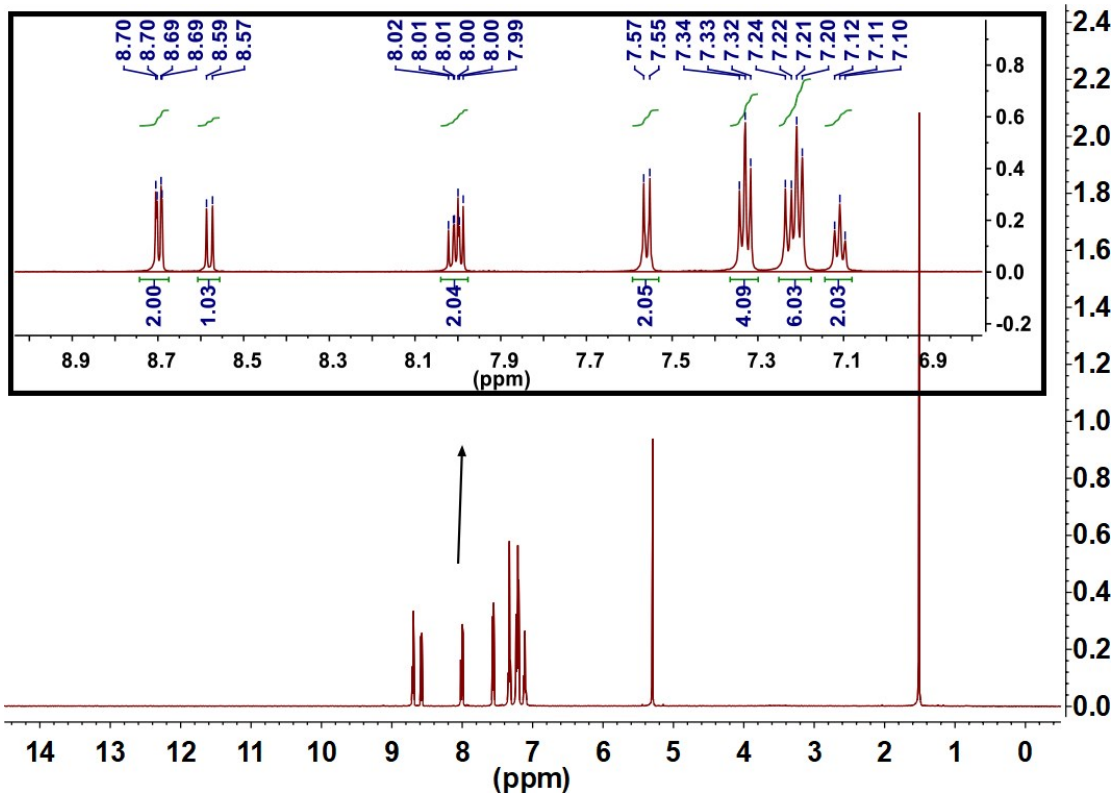

Fig. S23. ^{1}H-NMR spectra of TPAAZ.

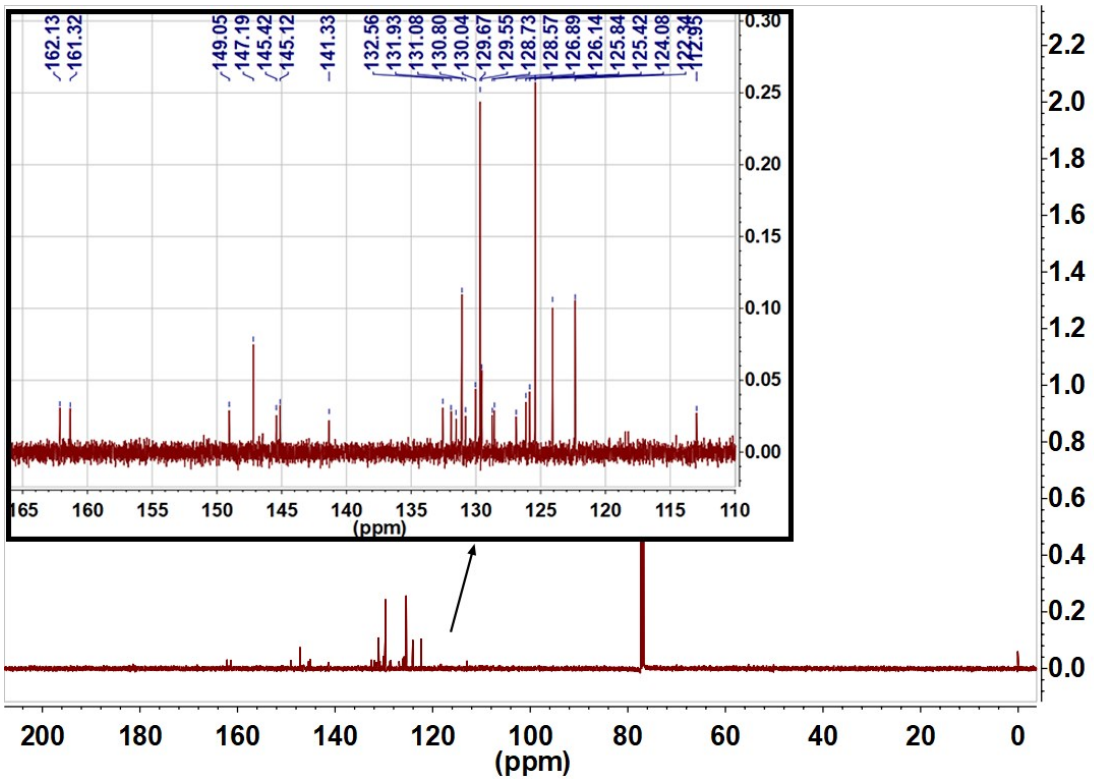

Fig. S24. ^{13}C-NMR spectra of TPAAZ.

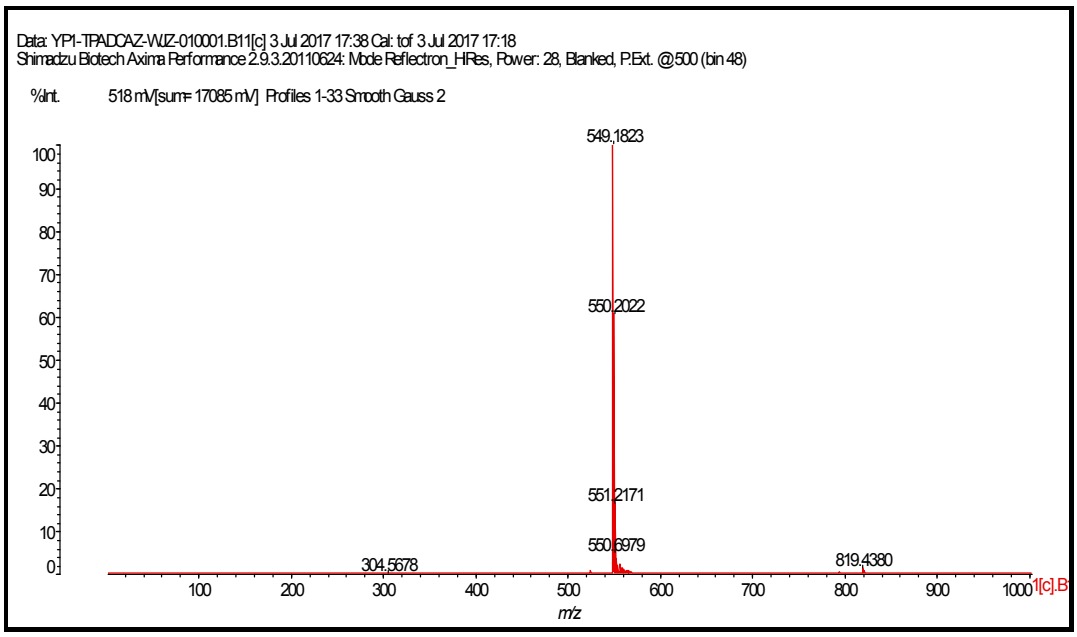

Fig. S25. MALDI-TOF-MS spectrum of TPAAZ.

References

1. J. Xue, Q. Liang, R. Wang, J. Hou, W. Li, Q. Peng, Z. Shuai and J. Qiao, *Adv. Mater.*, 2019, **31**, 1808242.
2. Q. Zhang, H. Kuwabara, W. J. Potscavage, S. Huang, Y. Hatae, T. Shibata and C. Adachi, *J. Am. Chem. Soc.*, 2014, **136**, 18070–18081.
3. H. Uoyama, K. Goushi, K. Shizu, H. Nomura and C. Adachi, *Nature*, 2012, **492**, 234–238.
4. Gaussian 16, Revision C.01, M. J. Frisch, G. W. Trucks, H. B. Schlegel, G. E. Scuseria, M. A. Robb, J. R. Cheeseman, G. Scalmani, V. Barone, G. A. Petersson, H. Nakatsuji, X. Li, M. Caricato, A. V. Marenich, J. Bloino, B. G. Janesko, R. Gomperts, B. Mennucci, H. P. Hratchian, J. V. Ortiz, A. F. Izmaylov, J. L. Sonnenberg, D. Williams-Young, F. Ding, F. Lipparini, F. Egidi, J. Goings, B. Peng, A. Petrone, T. Henderson, D. Ranasinghe, V. G. Zakrzewski, J. Gao, N. Rega, G. Zheng, W. Liang, M. Hada, M. Ehara, K. Toyota, R. Fukuda, J. Hasegawa, M. Ishida, T. Nakajima, Y. Honda, O. Kitao, H. Nakai, T. Vreven, K. Throssell, J. A. Montgomery, Jr., J. E. Peralta, F. Ogliaro, M. J. Bearpark, J. J. Heyd, E. N. Brothers, K. N. Kudin, V. N. Staroverov, T. A. Keith, R. Kobayashi, J. Normand, K. Raghavachari, A. P. Rendell, J. C. Burant, S. S. Iyengar, J. Tomasi, M. Cossi, J. M. Millam, M. Klene, C. Adamo, R. Cammi, J. W. Ochterski, R. L. Martin, K. Morokuma, O. Farkas, J. B. Foresman, and D. J. Fox, Gaussian, Inc., Wallingford CT, 2016; A. J. Becke, *Chem. Phys.*, 1993, **98**, 5648–5652; C. Lee, W. Yang and R. G. Parr, *Phys. Rev. B*, 1988, **37**, 785–789.
5. T. Lu and F. Chen, *J. Comput. Chem.*, 2012, 33, 580–592; T. Lu, F. Chen. Acta *Phys. Chim. Sin.*, 2012, 28(01): 1-18.

6. Dalton, a molecular electronic structure program, Release 2018.2 (2018), see http://daltonprogram.org; K. Aidas, C. Angeli, K. L. Bak, V. Bakken, R. Bast, L. Boman, O. Christiansen, R. Cimiraglia, S. Coriani, P. Dahle, E. K. Dalskov, U. Ekström, T. Enevoldsen, J. J. Eriksen, P. Ettenhuber, B. Fernández, L. Ferrighi, H. Fliegl, L. Frediani, K. Hald, A. Halkier, C. Hättig, H. Heiberg, T. Helgaker, A. C. Hennum, H. Hettema, E. Hjertenaes, S. Høst, I.-M. Høyvik, M. F. Iozzi, B. Jansík, H. J. Aa. Jensen, D. Jonsson, P. Jørgensen, J. Kauczor, S. Kirpekar, T. Kjaergaard, W. Klopper, S. Knecht, R. Kobayashi, H. Koch, J. Kongsted, A. Krapp, K. Kristensen, A. Ligabue, O. B. Lutnaes, J. I. Melo, K. V. Mikkelsen, R. H. Myhre, C. Neiss, C. B. Nielsen, P. Norman, J. Olsen, J. M. H. Olsen, A. Osted, M. J. Packer, F. Pawlowski, T. B. Pedersen, P. F. Provasi, S. Reine, Z. Rinkevicius, T. A. Ruden, K. Ruud, V. V. Rybkin, P. Sałek, C. C. M. Samson, A. S. de Merás, T. Saue, S. P. A. Sauer, B. Schimmelpfennig, K. Sneskov, A. H. Steindal, K. O. Sylvester-Hvid, P. R. Taylor, A. M. Teale, E. I. Tellgren, D. P. Tew, A. J. Thorvaldsen, L. Thøgersen, O. Vahtras, M. A. Watson, D. J. D. Wilson, M. Ziolkowski and H. Ågren, WIREs Comput Mol Sci, 2014, 4, 269–284.
7. Tian Lu, Multiwfn Manual, version 3.7(dev), available at http://sobereva.com/multiwfn/misc/Multiwfn_3.7_dev.pdf. (a) Section 3.21.1.1 Page 194-198. (b) Section 3.21.8, Page 217-219. (c) Section 3.21.A, Page 192. (d) Section 4.18.8.1, Page 637-638.
8. (a) Mrs. Sima Abdollahi, E. Nemati-Kande and A. Poursattar Marjani, ChemistrySelect, 2020, 5, 3971–3980; (b) D. Zhao, R. M. Saputra, P. Song, Y. Yang, F. Ma and Y. Li, Solar Energy, 2020, 201, 872–883; (c) J. Liu, Y. Zhang, K. Zhang, J. Fan, C.-K. Wang and L. Lin, Organic Electronics, 2019, 71, 212–219.